

# The kinematics of the planetary nebula BD+30°3639

Myfanwy Bryce<sup>1</sup> and Garrelt Mellema<sup>2</sup>

<sup>1</sup>*Department of Physics and Astronomy, The University of Manchester, Oxford Road, Manchester M13 9PL, UK;*  
*email: mbryce@ast.man.ac.uk*

<sup>2</sup>*Stockholm Observatory, SE-13336 Saltsjöbaden, Sweden;*  
*email: garrelt@astro.su.se*

Accepted 1999 — Received 1998 —

## ABSTRACT

In this paper we describe the results of the first optical kinematic study of the planetary nebula BD+30°3639. This system has a central star of the Wolf-Rayet type and is believed to be fairly young. Emission line spectra were obtained at high spectral and spatial resolution using the Utrecht echelle spectrometer at the William Herschel Telescope. These spectra indicate that the main ionized shell of BD+30°3639 appears to be evolving in a more complex way than previously thought.

**Key words:** planetary nebulae: individual: BD+30°3639 – interstellar medium: kinematics and dynamics

## 1 INTRODUCTION

The planetary nebula (henceforth PN) BD+30°3639 (PN G064.7+05.0) is a compact, young PN with a Wolf-Rayet type central star. Its surface brightness is among the highest of all PNe and the object has been intensively studied at many wavelengths; from X-rays (Arnaud, Borkowski & Harrington 1996), optical (Harrington et al. 1997), infrared (Latter et al. 1995; Siebenmorgen, Zijlstra & Krügel 1994), millimeter (Bachiller et al. 1991) to radio (Bryce et al. 1997a), to name only a few of the many references.

It is believed to be young because of the low effective temperature of the star ( $\sim 40\,000$  K) and low expansion age of the nebula. The central star is special in that it shows a hydrogen-deficient, Wolf-Rayet type spectrum (type [WC9]). The stellar spectrum was analysed by Leuenhagen, Hamann & Jeffrey (1996) who derived a surface temperature ( $T_{2/3}$ ) of 42,000 K, a luminosity,  $\log_{10} L = 4.71$ , a mass loss rate of  $1.3 \times 10^{-5} M_{\odot} \text{ yr}^{-1}$ , and a wind velocity of  $700 \text{ km s}^{-1}$ .  $L$  and  $\dot{M}$  are distance dependent, and these authors assumed a distance of 2.68 kpc to the central star (see below). As usual with winds from WR type stars, BD+30°3639's wind is rather massive.

Its distance has been determined using the expansion proper motions. Two groups used 6 cm *VLA* images combined with the optical expansion velocity from the literature to determine the distance. The reported distances are  $2.8^{+4.7}_{-1.2}$  kpc (Masson 1989),  $2.680 \pm 0.810$  kpc (Hajian, Terzian & Bignell 1993), and  $1.5 \pm 0.4$  kpc (Kawamura & Masson 1996). These distances are substantially larger than the previously derived distances using statistical methods, which lie mostly in the 600 to 700 pc range (Acker et al.

1992). Although the proper motion distances should be more reliable they are somewhat uncomfortable from the point of view of the evolutionary status of BD+30°3639. With a distance of 2.68 kpc, its luminosity would be around  $50,000 L_{\odot}$ , highest among PNe. Such a high luminosity would imply a massive ( $> 1.2 M_{\odot}$ ) central star, which would evolve on very short time scales ( $< 100$  years), something which has not been observed. Then again none of the published stellar evolution models apply directly to WR-type central stars.

BD+30°3639 is reported to have some more peculiar properties, such as a CO expansion velocity substantially higher ( $50 \text{ km s}^{-1}$ ) than that measured in any other species including  $\text{H}_2$  (Bachiller et al. 1991; Shupe et al. 1998). It also shows signs of both C and O-rich dust, the star itself being C-rich (Waters et al. 1998).

Although BD+30°3639 has been extremely well studied, to date no systematic kinematic study of the classical optical nebular lines has been done, perhaps partly because of the nebula's small size ( $6'' \times 4''$ ). However, the kinematics are an important element in understanding the PN. They can be used to help in deprojecting the object, are also essential in converting the observed proper motions into distances, and can help in the interpretation of the kinematics observed at other wavelengths (such as  $\text{H}_2$  and CO). In this paper we report on the first long slit spectroscopy of BD+30°3639.

The lay-out of the paper is as follows: the observations and data analysis are described in Sect. 2, in Sect. 3 we discuss and interpret the results, and we sum up our conclusions in Sect. 4.

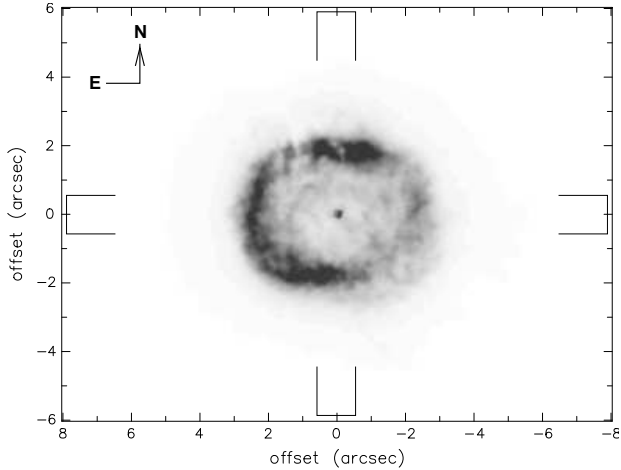


**Figure 1.** The HST narrow band  $H\alpha$  image of BD+30°3639 (Harrington et al. 1997) with the EW and NS slit orientations indicated.

## 2 OBSERVATIONS AND DATA ANALYSIS

High dispersion, spatially resolved spectra were obtained from BD+30°3639 using the William Herschel Telescope (WHT) on La Palma combined with the Utrecht echelle spectrometer (UES) and the Tek1 CCD detector. The observations were made on 1994 August 20 and 21. UES was used with the 79 grooves  $\text{mm}^{-1}$  grating and the maximum slit length of  $15''$ , long enough to cover the main shell of BD+30°3639. However, the wide inter-order separation which permits use of a relatively long slit also means that full order coverage is not possible with the  $1024 \times 1024$  pixel Tek1 CCD. Therefore, each slit position was observed at two grating positions, covering either end of the 31<sup>st</sup>–45<sup>th</sup> orders ( $4740 \text{ \AA} - 7415 \text{ \AA}$ ) which include most of the bright, kinematically and diagnostically useful optical emission lines. A slit width of  $252 \mu\text{m}$  ( $\equiv 1.12''$ ) was used; this is matched to two detector pixels (each  $24 \mu\text{m} \times 24 \mu\text{m}$ ), giving a velocity resolution of  $6.12 \text{ km s}^{-1}$ . In the spatial direction (with the derotator), the scale at the detector is  $14.96'' \text{ mm}^{-1}$ , so that 1 pixel  $\equiv 0.36''$ . The ‘seeing’ remained consistent at  $\sim 1''$  throughout the observing period.

The main ionized structure of this PN is remarkably rectangular in appearance with its major and minor axes aligned approximately along the EW and NS directions respectively (Fig. 1). Data were obtained from several slit positions aligned NS and EW across the nebula. A Thorium-Argon wavelength calibration spectrum was obtained at each slit and grating position. Flat-field frames were obtained using a quartz lamp and a wide slit ( $\equiv 5''$ ) exposure of the flux standard star SP 1942+261 was also obtained at each grating position.

When these observations were obtained, the A&G system on the UES was not fully operational and it became apparent after the data reduction process that we could only be absolutely certain of the spatial positions of the three runs which were clearly centred on the central star (Table 1).

The advantage of obtaining data from several prominent emission lines in one exposure was largely cancelled out by the loss of data due to positional uncertainty and the much longer timescale required for the non-standard re-

**Table 1.** Observational Data

	run 1	run 2	run 3
slit orientation	E-W	N-S	N-S
exp time (s)	600	60	600
emission lines (* - saturated)	*[N II]6584 Å *Hα He I 5876 Å [N II]5754 Å [N I] 5198+5200 Å [O III]5007 Å Hβ	[N II]6584 Å Hα He I 5876 Å [N II]5754 Å [N I] 5198+5200 Å [O III]5007 Å Hβ	[S II]6716+6731 Å *Hα [N II]6548 Å [O I]6364 Å He I 5876 Å [O III]4959 Å Hβ

duction process. These factors should be considered if future observations of this type are undertaken.

### 2.1 Data reduction

The initial processing was done using standard IRAF routines to debias the data and calibration frames and to combine multiple exposures using standard cosmic ray rejection algorithms. No dark frames were obtained since the Tek CCD has a very low dark current. The remainder of the processing was done using STARLINK routines. The data were flat fielded in the usual way before the individual position-velocity (pv) arrays were extracted and wavelength calibrated. This part of the reduction process was non-standard and is described in Appendix A. Although some scattering was apparent in the inter-order separations around the bright emission lines, this was not removed since the 2-d nature of the spectra made it difficult to generate an accurate model for subtraction. The scattering is at a relatively low level and does not affect the kinematical interpretation of the spectra significantly. Finally the spectra were flux calibrated and the spectrum of the central star was removed from the pv arrays (Appendix B).

### 2.2 The main kinematical features

Examples of the spatially resolved [O III] and [N II] emission line profiles obtained after the reduction process from the NS and EW slits are given in Fig. 2. The wavelength axis on each image has been converted to radial velocity offset from the systemic velocity  $v_{\text{sys}}$  which was chosen to correspond to a heliocentric velocity of  $-32 \text{ km s}^{-1}$ . The spatial scale on each image has been converted to an offset in arcseconds from the position of the central star. In each case, the stellar spectrum has been subtracted from the data frame (Appendix B). As noted previously, it became clear when the data was analysed that the absolute slit positions of several of our observations could not be determined. Although we obtained unsaturated [N II]5754 Å data at both slit orientations, this line is intrinsically faint and so we prefer to show the much brighter [N II]6548 Å pv array obtained in run 3 in Fig. 2a) rather than the [N II]5754 Å pv array obtained in run 2. Although the relative brightnesses of these two emission lines depends on the electron density of the emitting gas, there is no significant difference between the shapes of the two pv arrays. Similarly, we obtained [O III]5007 Å data at both E-W and N-W slit positions but again this line is

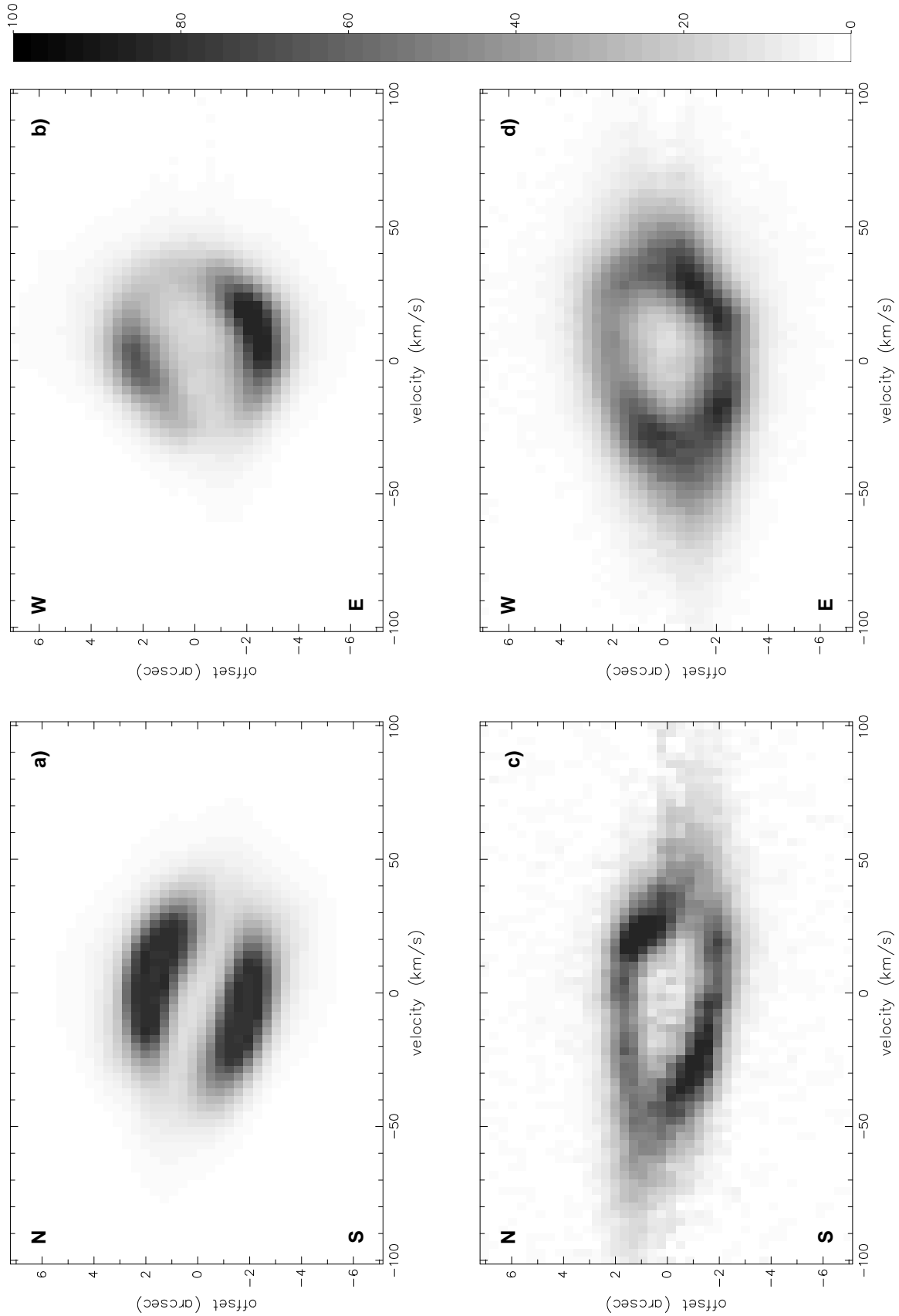


**Figure 2.** The two-dimensional position-velocity arrays of the (a)[N II]6548 Å (0–5000), (b)[N II]5754 Å (0–100), (c)[O III]4959 Å (0–15) and (d)[O III]5007 Å (0–36) emission obtained from runs 1 and 3. The scale bar corresponds to the ranges indicated, which are in units of mJy per pixel.

intrinsically weak and the short exposure time for the N-S position (run 2) gave a very noisy profile. Hence we prefer to show the [O III]4959 Å pv array obtained with a longer exposure time (run 3) in Fig. 2c). There is no problem in the direct comparison of these two lines as the [O III]5007 Å and [O III]4959 Å emission lines occur in the ratio of 3:1.

The main [N II] shell of emission is more spatially extended but less spectrally extended than the main [O III] shell. The velocity ellipses in both high and low ionizations and from both spatial directions are tilted with respect to the spectral axis and indeed the [N II] velocity ellipses appear to be almost open ended, with [O III] emission emerging from these gaps.

The NS and EW slit orientations were chosen because these are the projected minor and major axes of the PN (see Fig. 1). For a cylindrically symmetric nebula, these projected axes coincide with the direction of the three-dimensional (equatorial) symmetry plane and the (rotational) symmetry axis. However, the spatio-kinematic line emission maps shown in Fig. 2 indicate that this may not be the case. The two slit positions show that the blue shifted component of the bright [N II] emission from the NE part of the nebula is absent and similarly the red shifted component is absent from the SE part of the nebula. However, high speed blue and red shifted components appear in the [O III] emission from the NE and SW regions respectively. Similar high speed components were also found in the [N II] pv arrays although these components are much fainter than the main [N II] features shown in Fig. 2. Since the spatial offsets of the fastest moving components are close to the centre of the nebula, this implies a low inclination angle of a prolate nebula. The implications of this are discussed further in Sect. 3.

An [S II]6716 Å/6731 Å ratio map was made from the data from the NS slit and is shown in Fig. 3, together with the [S II]6731 Å position-velocity array. Note that the [S II]6731 Å pv array shows the same open ended velocity ellipse structure as that seen in the [N II]6548 Å pv array shown in Fig. 2a). The [S II]6716 Å/6731 Å intensity ratio (at a temperature of 10 000 K), varies from  $\sim 1.45$  to  $\sim 0.45$  over an electron density range of  $\sim 10 - 10^5 \text{ cm}^{-3}$  (Osterbrock 1989). The ratio map shows that there is a real variation in electron density around the velocity ellipse, with the apparently brightest parts having electron densities  $> 2 \times 10^4 \text{ cm}^{-3}$ , dropping to  $3 - 7 \times 10^3 \text{ cm}^{-3}$  at the fainter ends. The very faint, higher speed, blue-shifted component apparently emanating from the northern opening displays an electron density  $< 1000 \text{ cm}^{-3}$ .

### 3 DISCUSSION

#### 3.1 Nebular morphology and deprojection

The appearance of the line shapes as presented in the previous section have some interesting implications for the interpretation of the morphology of the nebula. We placed the slits along the projected minor and major axes of the nebula, which in the case of an inclined, cylindrically symmetric nebula would result in a skewed velocity ellipse along the major axis and a symmetric velocity ellipse along the minor axis. Our results show this not to be the case. Con-

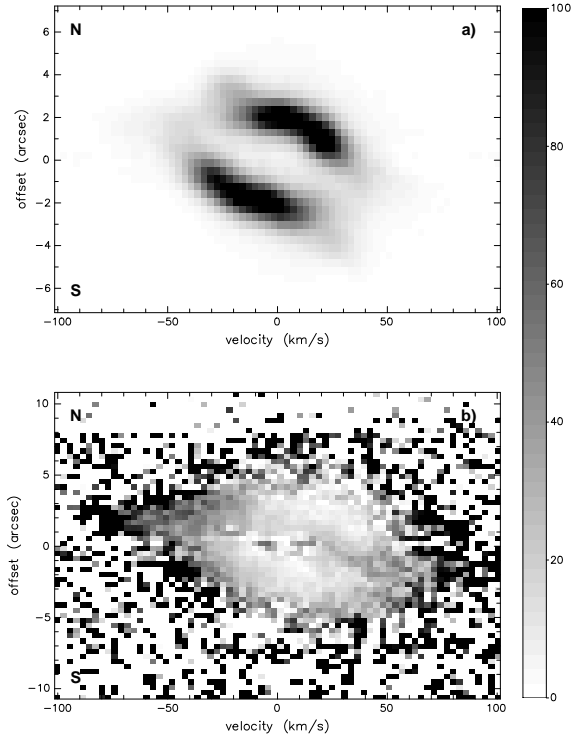


**Figure 3.** (a) Position velocity array of the [S II]6731 Å emission, scaled between 0 and 200 mJy/pixel. (b) [S II]6716 Å/6731 Å ratio map scaled between 0.4 and 0.8. The scale bar corresponds to these ranges.

sidering the *HST* and *VLA/MERLIN* images one may question whether BD+30°3639 is cylindrically symmetric since it looks more like a rounded off rectangle, something which appears to be inconsistent with any kind of projection of a cylindrically symmetric shell (Bryce et al. 1997a; Harrington et al. 1997). However, even with this boxy shape one would expect the line shapes to contain some information about the orientation of the bubble. Combining the NS and EW slits shows that the highest redshifts are found in the SW and the highest blueshifts in the NE part of the nebula. The most straightforward interpretation is then that the (rotational) symmetry axis of the nebula runs more or less diagonally across it roughly from NE to SW, with the NE side approaching us.

The brightness distribution in the line shapes, as well as the electron densities derived from the [S II]6716 Å/6731 Å intensity ratio show that the fastest parts of the PN also have the lowest densities, which is consistent with the picture of a prolate nebula with faster, low density polar regions. The morphology of BD+30°3639 combined with shape of the lines shows that we are seeing the nebula almost pole-on. Similar line shapes lead to this conclusion in the case of the Ring Nebula NGC 6720 (Bryce, Balick & Meaburn 1994). Further evidence comes from a comparison with the model line shapes based on hydrodynamic simulations presented in Chapter 5 of Mellema (1993) and the simple ellipsoidal model based on the distribution of the radio flux (Masson 1989), which gave a best fit inclination of 18° (but note that he assumed the rotational symmetry axis to run EW). We do

not think that the low spatial resolution of the data justifies more detailed kinematic modelling than this.

This ‘deprojection’ is supported by some other observations. As was pointed out in Bryce et al. (1997a) the smooth extinction gradient across the nebula (as derived from comparing high resolution optical and radio emission, see also Harrington et al. (1997)), can also be interpreted as being due to inclination. Assuming that most of the dust is located in a halo surrounding the entire optical nebula, or in an equatorial torus, and that the near side of the nebula is the NE, one would expect higher dust extinction in the SW, as is observed. The high extinction clump seen in the north-eastern part could then be lying along the rotational symmetry axis and be the feature in *BD+30°3639* which lies closest to us.

Graham et al. (1993) reported the detection of an  $H_2$  blob NE of the main optical nebula which was confirmed by Shupe et al. (1998). There is some indication of a structure at that position in the *HST* [S II]/ $H\alpha$  ratio map presented by Harrington et al. (1997). Sahai & Trauger (1998) present the *HST* data in a way which shows the faint small scale structures in the halo of *BD+30°3639*. Here one sees radial structures in the SW part of the halo and perhaps a smoother structure in the NE part. Although none of these observations individually could support the claim that we are seeing a prolate nebula almost pole-on with the rotational symmetry axis running NE-SW, combined this seems to be the most likely interpretation.

Comparing our new optical kinematic data to the  $H_2$  1-0  $S(0)$  data in Shupe et al. (1998), we do encounter a problem. Basically these authors find the opposite kinematic behaviour to that exhibited in our data: the  $H_2$  emission to the east of the nebula is red-shifted by up to  $30 \text{ km s}^{-1}$  with a faint component reaching  $60 \text{ km s}^{-1}$  and that to the west is blue-shifted, again by up to  $30 \text{ km s}^{-1}$  from the systemic velocity. However, our faint, high speed optical components are blue-shifted towards the east and red-shifted towards the west (the ionized gas at the eastern and western edges of the main optical shell is moving almost tangentially to the line-of-sight). We checked our slit orientation carefully and communicated with the authors of the other paper and the effect seems to be genuine. The explanation could be that the  $H_2$  lies in an expanding flattened structure around the prolate nebula, in which case it would be possible to see both positive and negative velocities along the same position angle, due to the effects of superposition along the line of sight. Such a scheme is illustrated in Fig. 4. The  $H_2$  map presented in Shupe et al. (1998) supports this interpretation since it shows a ring-like distribution around the ionized nebula. If this is the case the expansion velocity of parts of this ring would have to be quite high: the projected expansion velocity is about  $30 \text{ km s}^{-1}$ , which with the estimated inclination angle leads to a physical expansion velocity which is 2 to 3 times higher. Unfortunately, the resolution of the  $H_2$  data is only  $50 \text{ km s}^{-1}$ , so it is difficult to compare the molecular and ionized kinematics one to one.

### 3.2 Ionization stratification

Already in narrow band images it can be seen that there is a difference between the low ([N II]) and high ([O III]) ionization regions of the nebula (Harrington et al. 1997):

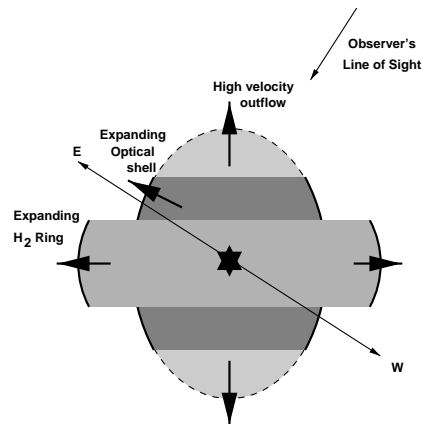


**Figure 4.** A sketch illustrating one possible scenario for the kinematical structure of *BD+30°3639*. Moving eastwards from the central star, the observer sees firstly the fast-moving, low density, optical emission along the approaching polar axis of the PN, then the lower ionization, bright optical emission from the main nebular shell expanding almost tangentially to the line of sight and finally the  $H_2$  emission from an outer ring of gas with a larger component of velocity along the line of sight.

the high ionization region is smaller than the low ionization region. The kinematic data show an even clearer difference. The high ionization lines are spatially less extended, reach much higher velocities and show a closed shell morphology, whereas the low ionization regions are indicative of an open ended shell (see Fig. 2). Combined with the deprojection suggested in the previous section this means that the prolate nebula has fast lower density polar caps which are faint in the low ionization lines, but relatively bright in the high ionization lines.

Masson (1989) suggested that *BD+30°3639* might be like NGC 7027, but seen pole-on. This was based on his simple ellipsoidal shell model. Because of the quite severe dust extinction in NGC 7027, it is difficult to compare optical narrow band images of the two nebulae. There is however a nebula which displays exactly the behaviour described in the previous paragraph, namely NGC 40. This nebula has an ellipsoidal shape with faint polar caps as seen in low ionization lines, whereas the high ionization lines show a closed shell. Another similarity between *BD+30°3639* and NGC 40 is that both have a WR-type central star, type [WC8] and [WC9] respectively (Leuenhagen et al. 1996).

When discussing the image and velocity data of NGC 40, Meaburn et al. (1996) suggested that the shells seen in [N II] and [O III] might have a different origin, the first one swept up by an ionization front, and the second by the fast wind from the WR-type central star. Nebulae of this type were found in the numerical models of Mellema (1995) and Mellema (1997). One expects such a configuration to occur early in the nebula’s evolution, which is consistent with *BD+30°3639*. The models show that one clear difference between the ionization and wind driven shells is that the first does not show much velocity variation as a function of latitude, whereas the latter does. In the case of NGC 40 the [O III] data were not available to test this hypothesis. For *BD+30°3639* we clearly observe higher velocities in the [O III] lines, supporting such a scheme. However, the size difference between the nebulae in the [N II] and [O III] im-

ages is rather marginal. As in the case of NGC 40 this means that the two shell scenario remains speculative.

### 3.3 Expansion velocities

BD+30°3639 is one of the radio brightest PNe and its distance has been measured by Kawamura & Masson (1996,  $900 \pm 200$  pc) and Hajian et al. (1993,  $2680 \pm 810$  pc), both using the observed proper motions of the expanding shell of ionized gas. In both cases the distance was calculated by combining the tangential motion derived from observations obtained at different epochs with the radial expansion velocity derived from optical emission line spectra. Both papers obtained an angular expansion rate of  $\sim 1.3$  mas yr $^{-1}$  for the outer edge of the minor axis, and both papers adopted an expansion velocity of 22 km s $^{-1}$ . However, Kawamura & Masson (1996) then included a correction for a constant flux assumption which explains the discrepancy between the final distance values. An expansion velocity of 22 km s $^{-1}$  was originally adopted by Masson (1989), in an earlier attempt to measure the distance to BD+30°3639, who made the point that good, spatially resolved kinematical data was not available at that time.

Our new data provide much more accurate expansion velocities. In Fig. 5, spectra from the two central crossections of the position-velocity arrays shown in Fig. 2(a) and (c) are presented. In each case the spectrum was fitted with Gaussian profiles and values for the radial expansion velocity observed at the centre of the nebula were derived from the centres of the two Gaussian components corresponding to the two main emission components. This gave values of  $28 \pm 1$  km s $^{-1}$  and  $35.5 \pm 1$  km s $^{-1}$  for the [N II] and [O III] profiles respectively. The value for the [O III] expansion is considerably higher than the value of 23 km s $^{-1}$  obtained by Sabbadin (1984). The explanation for this discrepancy probably lies in the fact that if such a measurement is made using lower spatial resolution (i.e. a wider slit or binning along the slit), the brighter, but radially slower moving components dominate the spectrum. Aller & Hyung (1995) obtained a value of  $\sim 26.8$  km s $^{-1}$  using a  $1.2'' \times 4''$  slit. In a simple proper motion measurement, the calculated distance to the object scales directly with expansion velocity, indicating that the distance measurements of Kawamura & Masson (1996) and Hajian et al. (1993) may have to be revised upwards. This would make the luminosity problem described in Section 1 even worse.

However, a serious problem for these types of distance calculation is that they are also dependent on a model which relates the radial expansion velocity to the observed tangential proper motions. If we are observing a prolate nebula almost pole-on, the discrepancy between the radial polar velocity and tangential equatorial proper motions is at its largest. This effectively means that the distances derived become upper limits. If the outer edge of the PN is actually an expanding ionization front (as suggested in Section 3.2), the relation between the radial gas velocity and the tangential proper motions becomes even more uncertain.

### 3.4 Evidence for a high-speed outflow

Harrington et al. (1997) presented several emission line ratio maps obtained from their WFPC2 images of BD+30°3639.

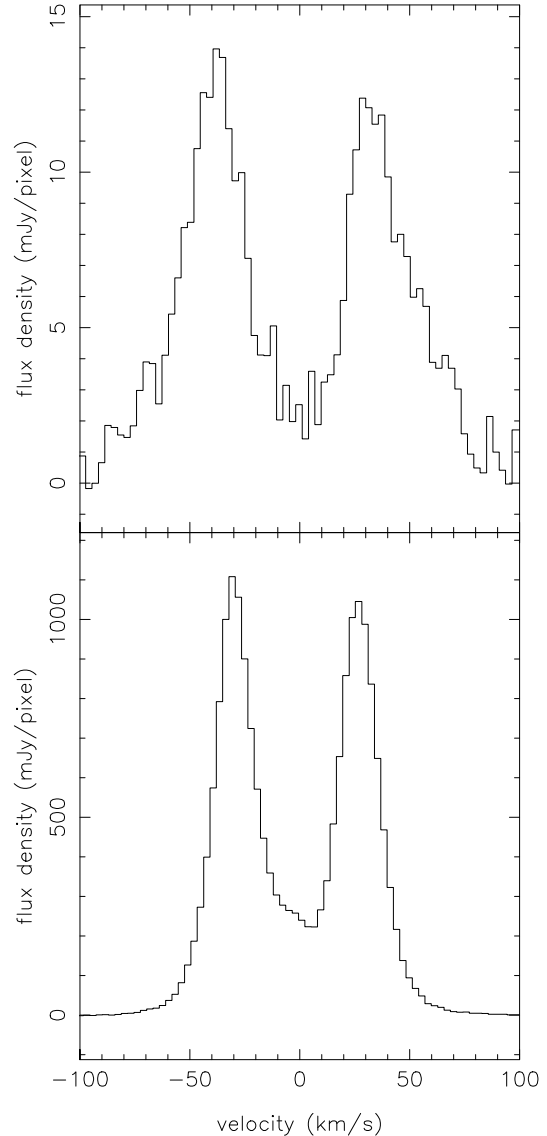


**Figure 5.** Spectra obtained by adding together the two central crossections from the NS slit for the [O III]4959 Å (upper) and [N II]6548 Å (lower) emission lines.

As mentioned above they discovered a compact ‘east blob’, particularly prominent in their [S II]/H $\alpha$  ratio map which is about twice as far from the centre of the nebula as the eastern limb of the main shell and coincides with the region of bright H $_2$  emission discovered by Graham et al. (1993).

Our data contains an interesting feature which could be associated with this ‘east blob’. The [N II]6584 Å emission line from the EW slit is shown in Fig. 6a, on a logarithmic scale chosen to show up the very faintest emission surrounding the main, bright, nebular shell (cf. Fig. 2b). The bright emission in this line from the main nebular shell saturated the CCD chip, but a faint feature extending towards the bottom left corner can be discerned. This feature lies at about 5–6'' east of the central star and has a velocity ranging from  $\sim -60$  to  $-90$  km s $^{-1}$ , much larger than the velocities exhibited by the main nebular shell. Also shown are data from

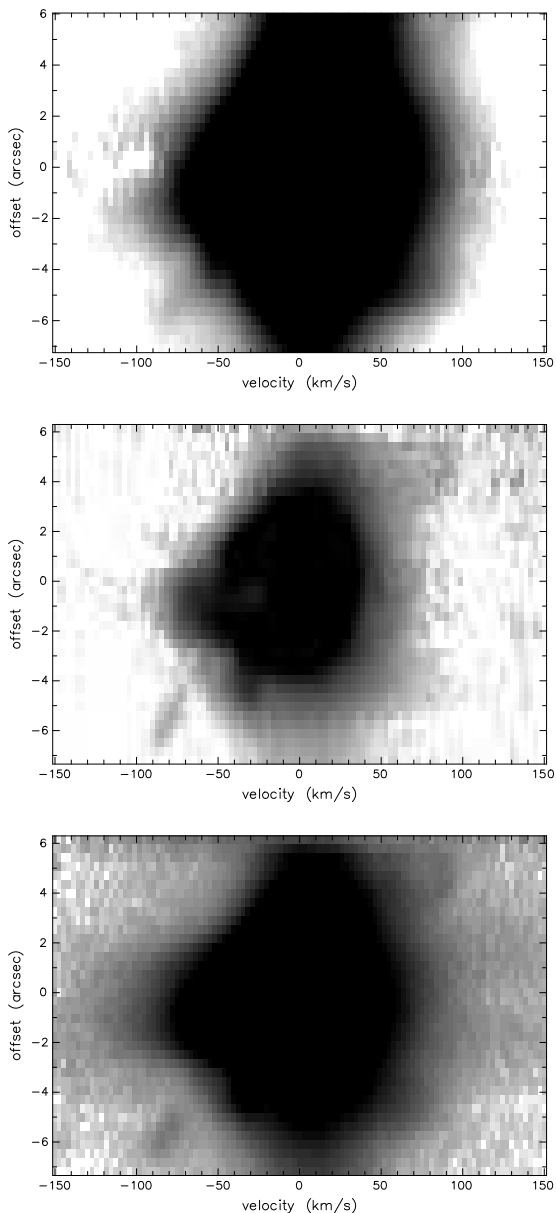


**Figure 6.** a) The p-v array of the [N II]6584 Å emission from the EW slit (run 1), showing a faint, accelerating flow to the east of the main nebular shell. b) The p-v array of the [S II]6731 Å emission obtained from an EW slit position offset slightly north of the central star; the accelerating flow is more prominent. c) The p-v array of the [N II]6548 Å emission from the same slit position as b).

another EW slit position, which was slightly offset (probably north) from the central star. The fast-moving feature appears very clearly in the [S II]6731 Å emission line (Fig. 6b) and also, though less prominently, in the [N II]6548 Å emission line (Fig. 6c). The intensity observed in the fast moving feature expressed as a fraction of the intensity in the brightest parts of the main shell was found to be approximately 5 times higher in [S II] than in [N II]6548 Å which is indicative of shock excitation. The [S II]6716 Å/6731 Å in the accelerating flow indicates an electron density  $< 850 \text{ cm}^{-3}$ .

Fast, low ionization features are often found outside the

main shells of more evolved PNe (e.g. FLIERS – Balick et al. 1993, BRETS – López, Meaburn & Palmer 1993) and recently very high speed features were observed around the young PN MyCn 18 (Bryce et al. 1997b). In most cases, such knots appear in pairs, on opposite sides of the central star, and in cases where more than one pair is observed there is often a point symmetry in the pattern. The feature in BD+30°3639 is only clearly seen on one side of the central star. Further observations are needed to establish the properties of this high velocity feature and to search for a possible counter-feature on the opposite side of the nebula.

In Bachiller et al. (1991;1992) it was noted that the CO outflow had a higher velocity than the optical outflow. Our data show this to be no longer true. The velocity of the feature discussed above reaches  $90 \text{ km s}^{-1}$ , and even in the main nebula these kinds of velocities are reached (see for example Fig. 2c). As noted above, the previously reported lower optical expansion velocities were based on measurements of the brighter parts of the nebula. The high velocity optical emission does seem to be strongly localised in the NE and SW. Bachiller et al. (1992) suggested two explanations for the observed CO spectrum: an expanding shell or two discrete bipolar blobs. They rejected the latter interpretation, but in view of our new results this should perhaps be reconsidered.

## 4 CONCLUSIONS

New, spatially resolved, high spectral resolution, position-velocity maps have been obtained in both high and low ionization emission lines from the young PN BD+30°3639. The low ionization data suggest a prolate, nearly axially symmetric, open-ended shape for the main nebular shell, with the rotational symmetry axis at about PA  $30^\circ - 60^\circ$  in the plane of the sky and an inclination of about  $20^\circ$ . The higher ionization material shows a closed shell structure of a somewhat smaller size. This structure may be similar to that seen in NGC 40. The high inclination makes it difficult to make the connection with the previously published image data, which show a remarkably rectangular shape for the main shell in both optical (Harrington et al. 1997) and radio continuum emission (Bryce et al. 1997a).

The velocity signature for the ionized material seems to be exactly opposite to that of the molecular material (Shupe et al. 1998): the eastern side is mostly blue-shifted in the ionized lines and red-shifted in the molecular lines. This behaviour can be explained if the molecular material sits in a flattened structure around the prolate nebula.

New estimates for the expansion velocity determined along the line of sight to the central star have been obtained,  $28 \pm 1 \text{ km s}^{-1}$  and  $35.5 \pm 1 \text{ km s}^{-1}$  for the [N II] and [O III] profiles respectively. These are higher velocities than previously supposed, probably because previous observations had a lower spatial resolution and therefore incorporated bright emission from the shell limbs which has a lower radial velocity. These new values can be of use in attempts to obtain the distance to BD+30°3639 using proper motion measurements (Kawamura & Masson 1996; Hajian et al. 1993). However, it should be kept in mind that the radial expansion velocity must be related to the tangential proper motions via a model

of the nebular structure and as noted above, our results indicate that a simple geometry may not be appropriate.

A fast moving ( $-90 \text{ km s}^{-1}$ ), faint feature was detected to the east of the main nebular shell. This feature may coincide with structure in the halo of BD+30°3639 detected by Harrington et al. (1997) in WFPC2 images and by Graham et al. (1993) from H<sub>2</sub> observations. This feature and the high velocity parts of the main shell have velocities close to twice as high as the reported CO velocity of  $50 \text{ km s}^{-1}$  (Bachiller et al. 1991).

## ACKNOWLEDGMENTS

The WHT is operated on the island of La Palma by the Isaac Newton Group in the Spanish Observatorio del Roque de los Muchachos of the Instituto de Astrofísica de Canarias. MB is in receipt of a Manchester University Research Fellowship. GM acknowledges support from the Swedish Natural Science Research Council (NFR). We would like to thank Dr Jeremy Walsh (STECF) for useful discussions on obtaining electron densities from the [S II]6716 Å/6731 Å ratio and for providing us with his program to calculate electron density at a given temperature for a given value of the ratio.

## REFERENCES

- Acker A., Ochsenein F., Stenholm B., Tylanda R., Marcout J., Schohn C., 1992, Strasbourg-ESO Catalogue of Galactic Planetary Nebulae. ESO, Garching.
- Aller, L.H., Hyung S., 1995, MNRAS, 276, 1102
- Arnaud K., Borkowski K.J., Harrington J.P., 1996, ApJ, 462, L75
- Bachiller R., Huggins P.J., Cox P., Forveille T., 1991, A&A, 247, 525
- Bachiller R., Huggins P.J., Martín-Pintado J., Cox P., 1992, A&A, 256, 231
- Balick B., Rugers M. Terzian Y., Chengalur, J. N., 1993, ApJ, 411, 778
- Bryce M., Balick B., Meaburn J., 1994, MNRAS, 266, 721
- Bryce M., Pedlar A., Muxlow T., Thomasson P., Mellema G., 1997a, MNRAS, 284, 815
- Bryce M., López J.A., Holloway A.J., Meaburn J., 1997b, ApJ, 475, L705
- Graham J. R., Herbst T. M., Matthews K., Neugebauer G., Soifer B. T., Serabyn E., Beckwith S., 1993, ApJ, 408, L105
- Hajian A. R., Terzian Y., Bignell C., 1993, AJ, 106, 1965
- Harrington J. P., Lane N. J., White S. M., Borkowski K. J., 1997, AJ, 113, 2147
- Kawamura J., Masson C., 1996, ApJ, 461, 282
- Latter W. B., Kelly D. M., Hora J. L., Deutsch L. K., 1995, ApJS, 100, 159
- Leuhenagen U., Hamann W.-R., Jeffrey C.S., 1996, A&A, 312, 167
- López J.A., Meaburn J., Palmer J.W., 1993, ApJ, 415, L135
- Masson C. R., 1989, ApJ, 346, 243
- Meaburn J., López J.A., Bryce M., Mellema G., 1996, A&A, 307, 579
- Mellema G., 1993, PhD thesis: Numerical models for the formation of aspherical planetary nebulae. Leiden University
- Mellema G., 1995, MNRAS, 277, 173
- Mellema G., 1997, A&A, 321, L29
- Osterbrock D.E., 1989, Astrophysics of Gaseous Nebulae and Active Galactic Nuclei, University Science Books, Mill Valley, California
- Sabbadin F., 1984, MNRAS, 209, 889
- Sahai R., Trauger J. T., 1998, AJ 116, 1357
- Shupe D. L., Larkin J. E., Knop R. A., Armus L., Matthews K., Soifer B. T., 1998, ApJ, 498, 267
- Siebenmorgen R., Zijlstra A.A., Krügel E., 1994, MNRAS, 271, 449
- Waters L. B. F. M., Beintema D. A., Zijlstra A. A. et al., 1998, A&A, 331, L61

## APPENDIX A: EXTRACTION AND CALIBRATION OF INDIVIDUAL ECHELLE ORDERS

Neither STARLINK nor IRAF contain specific packages for reducing cross-dispersed echelle spectra in the case where the 2-d structure of the emission line profiles are to be preserved. This is because, spatially extended, cross-dispersed spectra are usually obtained for point-like sources and the extended slit thus permits accurate sky subtraction, a process which is folded into the standard reduction packages which then produce a 1-d spectrum of the target. The first problem with cross-dispersed echelle data is to straighten the orders. Each order appears as an approximately vertical stripe in the raw CCD frame but each ‘stripe’ is at a slight angle to the next one. It is desirable to rebin the data such that the ‘stripes’ become exactly parallel. The largest angle between an order and the y-axis was  $0.87^\circ$ , equivalent to a shift of 15.5 pixels along the x-axis from the first cross-section to the last. The amount of rotation required to straighten the orders was found to be too small for standard rotation routines which did not handle the rebinning of data sufficiently accurately. The orders were straightened using routines which are usually used to SCRUNCH (wavelength calibrate) data. We used the continuum spectrum from the standard star as a pseudo-calibration arc. This continuum spectrum traces out a set of approximately vertical lines. Each ‘arc line’ was identified with the horizontal position (‘rest wavelength’) of the continuum spectrum in that order in the vertically central cross-section of the CCD frame, using the ARC2D routine from the TWODSPEC package in STARLINK. A dispersion calibration file was then produced. This file was used to ‘SCRUNCH’ the other data files, resulting in a set of CCD frames containing parallel echelle orders. The CCDEDIT and TRANNDF routines from the CCDPACK package were used to extract and rotate (through  $90^\circ$ ) each order of interest such that wavelength increases from left to right, resulting in a set of pv arrays, each with the central star at the same spatial position.

The PN data frames and standard star frames for each order were then wavelength calibrated, following the normal wavelength calibration procedure for longslit spectra, using the Th-Ar calibration spectra and the routines ARC2D and ISCRUNCH. Finally, each PN data frame was corrected for air-mass and flux calibrated using standard FIGARO routines. The flux calibration is not entirely rigorous for a variety of reasons, primarily because only one wide-slit exposure of the flux standard was obtained each night (i.e. one for each grating position), although the observing conditions were stable. Moreover, the flux calibration is based on an interpolated spectrum derived from calibrated data points spaced at intervals of less than one per observed wavelength range in a single order. Orders which contain prominent permitted



transitions such as  $H\alpha$  and  $H\beta$ , show wide absorption profiles in the standard star spectrum; these profiles may extend further than the limits of the observed wavelength range in that order and so may not have been properly corrected for. Nevertheless, the internal consistency appears to be good, for example the total fluxes in the  $H\alpha$  and  $H\beta$  lines, which appear in the spectra from both grating positions, were consistent to within 5% and comparison of the total flux in the  $[\text{N II}]6584 \text{ \AA}$  emission line which appeared at grating position 1 with that in the  $[\text{N II}]6548 \text{ \AA}$  emission line observed at grating position 2 showed that the ratio of fluxes was within 6% of the theoretical ratio of 3:1. The absolute flux calibration was also found to be consistent with other observations. An estimate of the total  $H\beta$  flux from the nebula, obtained by considering the total flux observed through a single slit and scaling up from the slit area to the nebular area, is  $8.4 \times 10^{-14} \text{ J s}^{-1} \text{ m}^{-2}$ . This rather crude estimate compares well with the values in Acker et al. (1992) ( $9.33 \times 10^{-14} \text{ J s}^{-1} \text{ m}^{-2}$ ) and Harrington et al. (1997) ( $10.5 \times 10^{-14} \text{ J s}^{-1} \text{ m}^{-2}$ ).

## APPENDIX B: STAR SUBTRACTION

The central star continuum has been subtracted from the pv arrays displayed in this paper, so that the nebular emission can be appreciated. This procedure is complicated by the fact that the central star of *BD+30° 3639* is a Wolf-Rayet type star with broad emission features superimposed on the continuum spectrum. The stellar emission features are about an order of magnitude broader than the nebular emission line features. The two spatial pixels containing the brightest part of the stellar spectrum were first extracted from the pv array of the order of interest. Any obvious nebular features were clipped out of this spectrum and the resulting spectrum was fitted with a polynomial function. The fitted function was grown back into a 2-d array. A spatial profile of the central star was obtained from the original pv array (from a region well away from any nebular emission) and this profile was used to modify the regenerated stellar pv array in the spatial direction. Finally this pv model for the stellar spectrum was normalised to the same flux scale as the original pv array by comparing the flux levels from the stellar continuum, again at a position well away from any nebular features. This pv array was then subtracted from the original array to leave just nebular emission. Careful analysis showed that small residuals appeared, corresponding to the extended wings of the stellar profiles at positions where broad stellar emission features had occurred, however, these were barely visible over the background noise level and we do not believe that they affect our analysis of the nebular data.